Defect and Diffusion Forum Vol. 364 (2015) pp 92-103 *Online: 2015-06-08*

doi:10.4028/www.scientific.net/DDF.364.92

Multi-scale Modeling of Internal Mass Diffusion Limitations in CO Oxidation Catalysts

J.E.P. Navalho[1,a], J.M.C. Pereira[1,b] and J.C.F. Pereira[1,c]

LAETA, IDMEC, Instituto Superior Técnico, Universidade de Lisboa, Mechanical Eng. Dept. / LASEF, Av. Rovisco Pais, 1, 1049-001 Lisbon, Portugal

[a]jorge.navalho@tecnico.ulisboa.pt, [b]jose.chaves@tecnico.ulisboa.pt, [c]jcfpereira@tecnico.ulisboa.pt

Keywords: Multi-scale modeling; effective diffusivity; intraporous diffusion limitations; reaction-diffusion modeling; digital media reconstruction; catalytic combustion

Abstract. This work applies a 3D multi-scale bottom-up approach for modeling the processes of diffusion and reaction-diffusion in porous catalyst layers. The performance of the random pore model to predict effective transport coefficients are compared with the results of the multi-scale diffusion model. The results of the 3D multi-scale diffusion model are employed in a 1D pseudo-homogeneous reaction-diffusion model with a relative good agreement with the 3D multi-scale reaction-diffusion model. Furthermore, the former multi-scale model was coupled to a full-scale reactor model with good results and high advantages in terms of computational time savings.

Introduction

The catalytic oxidation of CO finds a great practical application in the after-treatment processes of exhaust gases from automobiles (catalytic converter) since the beginning of the environmental concerns and the first environmental regulations dated back to the 70's of the last century [1]. Several catalyst formulations have been considered suitable for performing the oxidation of CO with high activity towards the total conversion product such as platinum group metals (namely Pt, Pd and Rh) combined with the high surface area alumina catalysts [1-2]. Due to the application of a catalytic porous layer (washcoat) onto the walls of a substrate (support) structure (commonly a honeycomb monolith in the automotive industry) to enhance the kinetic rates, intraporous diffusional limitations can be observed depending on the operating condition, catalyst activity and porous layer structural properties [3]. Neglecting mass gradients along the catalyst layer, driven by diffusion limitations, in a model that predicts the overall performance of a catalytic converter may strongly affect the prediction capability of such a model even for thin washcoat layers [4-5].

To include the effect of mass transfer resistance along the washcoat layer in a full-scale reactor model several techniques have been employed. The less demanding strategy consists in the evaluation of effectiveness factors with the Thiele modulus. Thiele modulus calculation is straightforward for the steady-state reaction-diffusion problem in an isothermal catalyst layer with constant catalyst activity, where the overall reaction scheme is described by a single-irreversible reaction defined with a first-order power rate law equation and the species transport are described by spatially-independent diffusion coefficients [3]. However, most often for non-first order power law kinetics or for other rate forms (such as the Langmuir-Hinshelwood type of rate expressions) or for reversible reactions, a generalized Thiele modulus is defined due to the absence of an analytical solution for the reaction-diffusion problem [3,6-7]. Other works solved the 1D/2D reaction-diffusion equations due to the complex set of reactions [5] or due to the washcoat geometry [8].

Other sophisticated strategies to properly take into account the pore diffusion limitations through the full solution of the reaction-transport equations have received growing attention in recent years. The digital reconstruction of the porous layer through stochastic [9] or semi-deterministic methods [10] or through high-resolution 3D imaging techniques [11] followed by the 3D pore-scale

numerical solution of the reaction-diffusion equations for each species in isothermal and non-isothermal conditions has been identified as a trend in the catalyst modeling community [12-13]. In particular, for bi-dispersed pore systems a strategy has been employed based on the decomposition of the physical model in two sub-models (multi-scale approach) each one being characteristic of the two length-scales followed by numerical simulations for each sub-model in the bottom-up direction. Under inert conditions several authors have applied such strategy to evaluate effective diffusivities in porous media [12,14]. Effective thermal conductivities have been also obtained through the same overall modeling strategy [15-16]. Under reacting conditions, the multi-scale approach was explored for CO oxidation in porous catalyst layers [17-18] and for methane steam reforming in a microstructured reactor [16].

In this work the application of a multi-scale methodology is considered to predict the performance of a catalyst porous layer under reacting and non-reacting conditions. Several strategies are discussed to include the effect of diffusional limitations in the full-scale reactor model for the prediction of the overall performance of a honeycomb reactor. These strategies include the pre-computation of averaged reaction rates with the 3D multi-scale reaction-diffusion methodology or through the 1D pseudo-homogeneous reaction-diffusion model with effective transport coefficients obtained through theoretical models or through the 3D multi-scale diffusion model.

The current manuscript is organized in seven sections. The first section is dedicated to the introduction. The second and third sections describe the mathematical formalism of the underlying phenomena and the numerical strategies employed to solve the mathematical models, respectively. Section four is devoted to the methodology considered for the computational reconstruction of the catalytic porous structures. A validation of the multi-scale methodology is thereafter presented (section five) as well as the discussion of its application to the evaluation of the performance of a CO honeycomb catalyst (section six). The paper ends with a brief summary of conclusions.

Mathematical Modeling

The application of the current multi-scale washcoat model allows the extraction of effective diffusion coefficients (transport model – under non-reacting conditions) in a specific porous layer and the evaluation of the internal transport limitations under reacting conditions (reaction-diffusion model). In particular, the multi-scale reaction-diffusion model can be coupled with full-scale reactor models, such as the 1D heterogeneous single-channel model, for the prediction of the overall (macro) reactor performance.

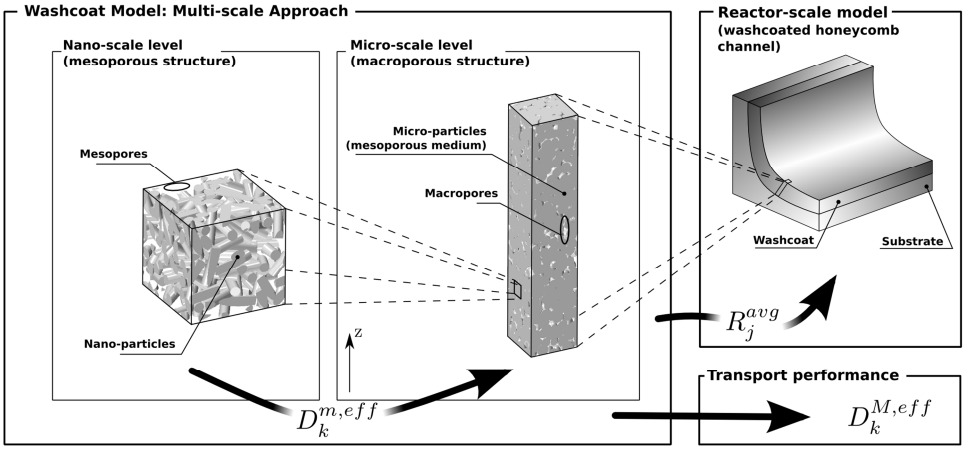

Fig. 1 – Overall multi-scale methodology and coupling strategy between different length-scales.

Porous catalytic layers characterized by a bimodal pore structure are under consideration in the current multi-scale washcoat model since this model takes into account two length-scale levels, the nano-scale and the micro-scale levels, representative of the small pores (mesopores – $\mathbf{2\ nm} < \boldsymbol{d_p} <$

$\mathbf{50\ nm}$) and large pores (macropores – $\boldsymbol{d_p > 50\ nm}$), as Fig. 1 illustrates. At the nano-scale level the solid fraction (nano-particles) is non-porous whereas at the micro-scale level the solid grains (micro-particles) are composed by the mesoporous structure considered in the nano-scale level. However, the transport steps within the micro-particle structure are mathematically considered through a pseudo-homogeneous approach, *i.e.*, the transport phenomena are modeled with effective transport properties (effective diffusion coefficients - $\boldsymbol{D_k^{m,eff}}$) evaluated in the nano-scale level and imported to the micro-scale level.

3D Multi-Scale Diffusion and Reaction-Diffusion Models. The objective of the diffusion model is the determination of effective diffusion coefficients, for a specific structure and specific operating conditions, for the whole porous layer. For the nano-scale level, the mathematical model is the same whenever the final objective is the evaluation of the effective transport coefficients or the determination of the extent of diffusional limitations. However, at the micro-scale level depending if the interest relies on the evaluation of effective transport data or averaged reaction rates, the mathematical model may not include a species source term physically justified by the species production/depletion due to chemical reactions promoted by the catalyst activity.

Nano-Scale (Diffusion) Model. At this scale, the species transport is predominantly governed by the Knudsen regime of diffusion due to the small pore radius in comparison with the molecules mean free path and consequently, bulk diffusion is neglected at this scale. At steady-state and isothermal conditions, the diffusion of each species in the pore space of mesoporous media (computational domain) is described by Eq. (1) provided that the continuum approach is still a valid assumption in this scale (see for instance [19]).

$$\nabla.\left(D_{k,K} c \nabla X_k\right) = 0 \tag{1}$$

In Eq. (1), $D_{k,K}$ corresponds to the Knudsen diffusion coefficient evaluated with Eq. (2) where r_p is the local pore radius, c is the mixture total molar concentration (considering an ideal gas mixture) and X_k is the molar fraction of species k.

$$D_{k,K} = \frac{2}{3} r_p(\boldsymbol{x}) \left(\frac{8RT}{\pi M_k}\right)^{1/2} \tag{2}$$

The system of equations derived by the application of Eq. (1) to all reactive gas species (CO, O_2 and CO_2) are subjected to Dirichlet boundary conditions in the z-direction, in order to impose species concentration differences in opposed faces ($c(X_k^1 - X_k^0)$), and to Neumann boundary conditions (zero species molar fluxes) in the x- and y-directions. After the achievement of a converged numerical solution for the species concentration field, the effective diffusion coefficient for each species can be evaluated through Eq. (3), where V_T^m is the total volume of the mesoporous structure (representative elementary volume – pore and solid space) and L is the distance between the two parallel boundaries in z-direction.

$$D_k^{m,eff} = \frac{1}{V_T^m} \int_{V_T^m} D_{k,K} c \frac{\partial X_k}{\partial z} dV \frac{L}{c(X_k^1 - X_k^0)} \tag{3}$$

For each mesoporous medium the procedure above is required to be performed just once since for other temperatures and/or species the effective diffusivities can be evaluated through Eq. (4).

$$D_j^{m,eff}(@T_2) = D_k^{m,eff}(@T_1) \sqrt{\frac{T_2 M_k}{T_1 M_j}} \tag{4}$$

Micro-Scale Diffusion and Reaction-Diffusion Models. The diffusion mathematical model applied to the micro-scale level is also described by Eq. (1). The overall methodology for the diffusion model at this scale to compute effective diffusion coefficients ($D_j^{M,eff}$) is analogous to the procedure developed for the nano-scale level. Although, at this level, the species transport are considered in the pore and solid space and therefore two regimes of species diffusion are considered depending on the actual position in the structure: the molecular diffusion regime is considered in the pore space (macro-pores) and the Knudsen regime is considered in the solid fraction (micro-particles) but modeled in a pseudo-homogeneous fashion with effective diffusivities ($D_k^{m,eff}$) imported from the nano-scale level simulations. In this work, bulk (binary) diffusion coefficients for each species in a N_2 diluting mixture are computed through the Fuller-Schettler-Giddings correlation [20] given by Eq. (5).

$$D_{k,b} = \frac{0.00143T^{1.75}}{P\sqrt{2/\left(1/M_k + 1/M_{\mathrm{N_2}}\right)}\left[(\Sigma_{\mathrm{v}})_k{}^{1/3} + (\Sigma_{\mathrm{v}})_{\mathrm{N_2}}{}^{1/3}\right]^2} \tag{5}$$

The reaction-diffusion mathematical model under isothermal and steady-state conditions is described by Eq. (6) where ν_k is the stoichiometric coefficient of species k ($= \mathrm{CO}, \mathrm{O_2}$ or $\mathrm{CO_2}$) in the single-step reaction scheme that describes the CO total oxidation in a $\mathrm{Pt/Al_2O_3}$ catalyst ($\mathrm{CO} + 1/2\,\mathrm{O_2} \rightarrow \mathrm{CO_2}$) and q_R corresponds to the rate-of-progress variable of such reaction. The Langmuir-Hinshelwood kinetic expression developed by Voltz *et al.* [2] was herein considered with kinetic parameter reported in [17].

$$\nabla.\left(D_{k,K} c \nabla X_k\right) + \nu_k q_R = 0 \tag{6}$$

To close the system of equations that represents the mathematical model applied to all reactive gas species, Neumann boundary conditions are considered at the washcoat/substrate interface while Dirichlet boundary conditions defining the external (surface) washcoat mixture condition (operating condition) are considered at the top face in the z-direction of the micro-scale physical model. In the remaining boundaries Neumann boundary conditions are applied to all reactive species.

For a specific operating condition, the extent of transport resistances in the overall structure is determined from the converged numerical solution of the reaction-diffusion model through the computation of the internal effectiveness factor with Eq. (7), where V_S^M is the total volume of the porous micro-particles and q_R^{bnd} is the rate-of-progress variable at external (surface) conditions.

$$\eta = \frac{1}{V_S^M q_R^{bnd}} \int_{V_S^M} q_R dV \tag{7}$$

1D Pseudo-Homogeneous Reaction-Diffusion Model – Classical Approach. This model is mathematically described by Eq. (8) and considers the whole washcoat layer as a continuum medium whose transport properties are described through averaged (effective) properties.

$$\frac{\partial}{\partial z}\left(c D_k^{M,eff} \frac{\partial X_k}{\partial z}\right) + \nu_k q_R = 0 \tag{8}$$

Several theoretical/empirical expressions are available in the literature to evaluate effective diffusivities. For bi-dispersed pore systems, the random pore model (RPM) proposed by Wakao and Smith [21] is generally considered (see Eq. (9)). Analogously to the previous assumptions, the Bosanquet equation was not employed to evaluate transition diffusion coefficients because in the

macro-pore network only the regime of volume diffusion is taken into account while in the mesoporous structure only the Knudsen diffusion regime is considered. It is worth noting that the mesoporosity ($\varepsilon^{m\prime}$) in the framework of the random pore model corresponds to the ratio of the total volume occupied by the mesopores to the total washcoat layer volume, *i.e.*, $\varepsilon^{m\prime} = \varepsilon^{m}(1-\varepsilon^{M})$ where ε^{m} is the porosity on a total mesoporous system volume basis.

$$D_k^{M,eff} = (\varepsilon^M)^2 D_{k,b} + (\varepsilon^{m\prime})^2 D_{k,K} + \frac{4[\varepsilon^M - (\varepsilon^M)^2]}{1/D_{k,b} + (1-\varepsilon^M)^2 / \left[(\varepsilon^{m\prime})^2 D_{k,K}\right]} \tag{9}$$

1D Heterogeneous Single-Channel Model (Full-Scale Reactor Model). This model is largely employed in the literature to describe the overall performance of fixed-bed catalytic reactors, such as the honeycomb monolith reactor (see [22-23]). The application of this model to a single channel of the whole honeycomb structure is able to predict the entire thermal and chemical performance of the reactor provided that specific assumptions are respected [24]. This model is a non-isothermal two-phase (heterogeneous) model since it considers mass and energy balances for the bulk gas phase and for the solid phase (substrate and washcoat). Therefore, Eqs. (10) and (11) correspond to the mass and energy balance equations for the bulk gas phase, respectively, whereas Eq. (12) is the mass balance equation for the thin film at the bulk gas/external wall interface and Eq. (13) is the energy balance equation for the solid phase (washcoat and substrate). These equations are written in terms of species mass fractions and for steady-state conditions.

$$A\varepsilon\rho_g u \frac{\partial Y_{k,g}}{\partial x} + \frac{\partial}{\partial x}\left(A\varepsilon\rho_g Y_{k,g} V_{k,g}\right) + A a_V \rho_g K_{mat,k}\left(Y_{k,g} - Y_{k,w}\right) = 0 \tag{10}$$

$$A\varepsilon\rho_g u C_{p,g} \frac{\partial T_g}{\partial x} - \frac{\partial}{\partial x}\left(A\varepsilon k_g \frac{\partial T_g}{\partial x}\right) + A\varepsilon\rho_g \sum_{k=1}^{KK_g} Y_{k,g} V_{k,g} C_{p,k} \frac{\partial T_g}{\partial x} + A a_V h\left(T_g - T_s\right) = 0 \tag{11}$$

$$a_V \rho_g K_{mat,k}\left(Y_{k,g} - Y_{k,w}\right) - \nu_k q_R \xi W_k = 0 \tag{12}$$

$$-\frac{\partial}{\partial x}\left(A k_{s,eff} \frac{\partial T_s}{\partial x}\right) - A a_V h\left(T_g - T_s\right) + A\xi \sum_{k=1}^{KK_w} \nu_k q_R H_k = 0 \tag{13}$$

At the inlet section of the reactor Dirichlet boundary conditions are applied to the gas phase balance equations whereas a zero-Neumann boundary condition is considered for the energy balance of the solid phase. At the outlet section Neumann boundary conditions are considered for all governing equations. More details about the model formulation can be found elsewhere [22-23].

Numerical Modeling

The 3D multi-scale diffusion and reaction-diffusion models were implemented in the STAR-CCM+ software (version 6). This commercial package was employed to model the CAD geometry, generate the mesh and to obtain a converged numerical solution. The segregated species model was used to solve Eqs. (1) and (6) for all reactive gas species being the errors lumped in the diluting gas species (N_2).

The 1D pseudo-homogeneous and isothermal reaction-diffusion model for the continuum description of the washcoat performance as well as the 1D heterogeneous single-channel model were implemented in an in-house version of the PREMIX software. The 1D heterogeneous single-channel model was largely validated in the past for different reactor configurations, catalyst formulations, operating conditions and fuels and more details about its numerical formulation and procedures to obtain converged and mesh-independent solutions can be found elsewhere [22-24].

Digital Media Reconstruction. In this work the superposed spheres method [25] was employed to computationally generate 3D porous structures in a discrete space (voxels) with structural and morphological properties of real porous catalyst structures. The method considers as input data from experimental measurements the grain size distribution and the porosity of the porous layer. This method, initially developed for spheres, was extended for cylinder-shaped particles for the reconstruction of the nano-scale physical model where the grain shape follows the cylinder geometry [17].

The method randomly distributes the particles (spheres or cylinders) in the total volume of the porous medium following the provided input data and considering three placement factors: the attachment factor, exclusion factor and border factor. The attachment factor controls the attachment level during the placement of a new particle in relation to an existing particle in the medium; the exclusion factor defines the level of sintering among the particles; and the border factor determines the volume extent of the particles boundary voxels that belongs to the solid phase. At the end of the reconstruction procedure, the reconstructed medium is represented by a volume phase function containing the information about the actual phase in each voxel.

Model Validation. The validation of the 3D multi-scale diffusion and reaction-diffusion models is herein considered for the case of CO total oxidation within a digital reconstructed bi-dispersed pore structure with the textural properties given in Table 1 and extracted from the reference [17].
In Figs. 2a and 2b the pore size distributions of the generated samples (mesoporous and macroporous structures, respectively) are presented and compared with the reference pore size distribution data reported in the literature [17]. At the nano-scale level (Fig. 2a), a mean pore radius equal to 6 nm is observed for both reconstructed structures. A good matching is concluded between the pore size distributions of the structures generated in this study and the reference structures.

The 3D multi-scale diffusion model was applied for the porous sample generated in this work and the results concerning the converged CO mole fraction fields at the nano-scale and micro-scale levels are presented in Figs. 3a and 3b. From the converged CO concentration fields the obtained effective diffusion coefficients for CO in the mesoporous and in the macroporous structures

Table 1 – Structural parameters required for the digitally reconstruction of the porous sample at both length-scale levels (nano- and micro-scale levels).

		Mesoporous Structure	Macroporous Structure
Grain Shape Parameters	Cylinder Length (L_c^m)	20 nm	–
	Cylinder Diameter (d_c^m)	10 nm	–
	Sphere Diameter (d_s^M)	–	2.4 μm
	Porosity ($\boldsymbol{\varepsilon^m, \varepsilon^M}$)	43%	25%
	Exclusion Factor ($\boldsymbol{F_E}$)	0.0	0.7
	System Size ($\boldsymbol{L_x \times L_y \times t}$)	$100 \times 100 \times 100$ nm^3	$10 \times 10 \times 50$ μm^3

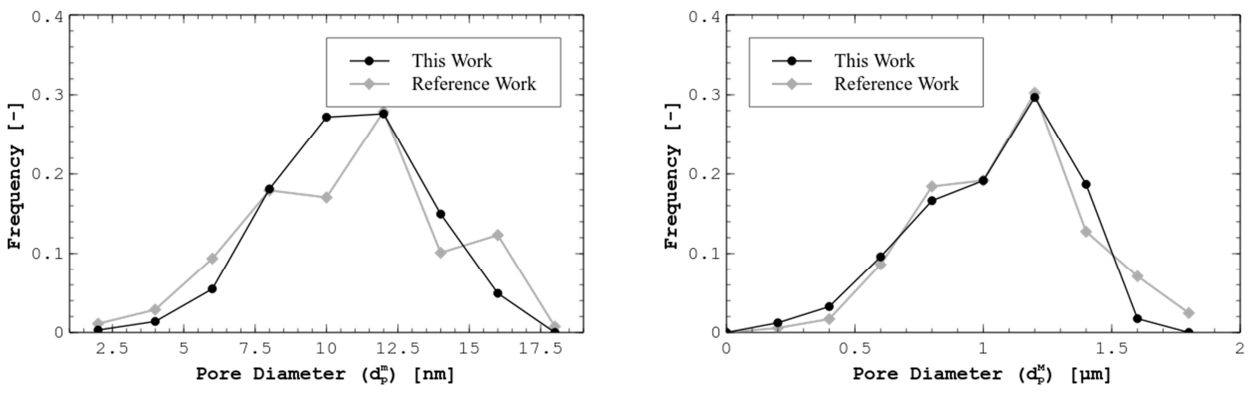

(a) **(b)**

Fig. 2 – Pore size distributions of the mesoporous structure (a) and macroporous structure (b) obtained in this work and reported in the reference work [17].

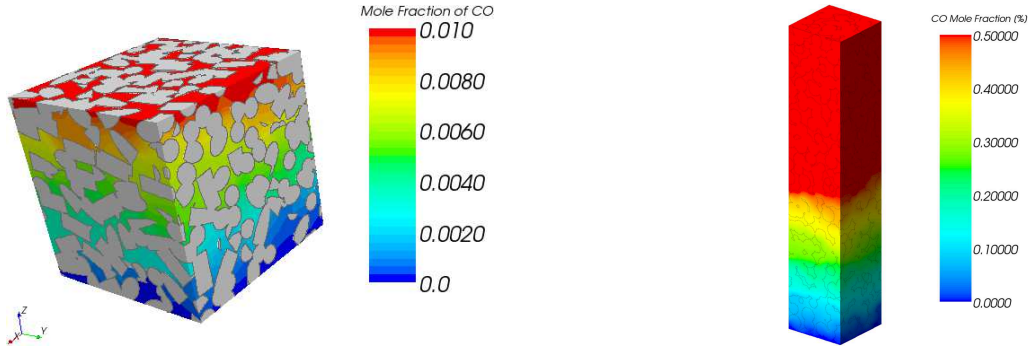

(a) **(b)**

Fig. 3 – CO mole fraction values plotted on the boundaries of the mesoporous (a) and macroporous (b) structures.

correspond to 3.6×10^{-7} m^2/s and 2.8×10^{-6} m^2/s, respectively. The predicted values slightly underestimate the values reported in the reference work by about 7.7% and 6.7% for the nano- and micro-scale levels, respectively. The slightly lower effective diffusivity values obtained in this work are strongly related with the small shift towards lower pore diameters observed in the pore size distribution of the generated mesoporous sample in relation to the pore size distribution of reference sample (see Fig. 2a). The comparison between the predicted results and the reference data for the 3D multi-scale diffusion model allows to conclude that this model is validated.

Finally, the validation of the 3D multi-scale reaction-diffusion model is carried out in the temperature range from 373 K to 623 K and for three different surface mixture compositions. The comparison between the predicted effectiveness factors and the effectiveness factors reported in the reference [17] is presented in Fig. 4. A general good matching between both sets of values is observed which reinforces the correct numerical implementation of the 3D multi-scale reaction-diffusion mathematical model formulation.

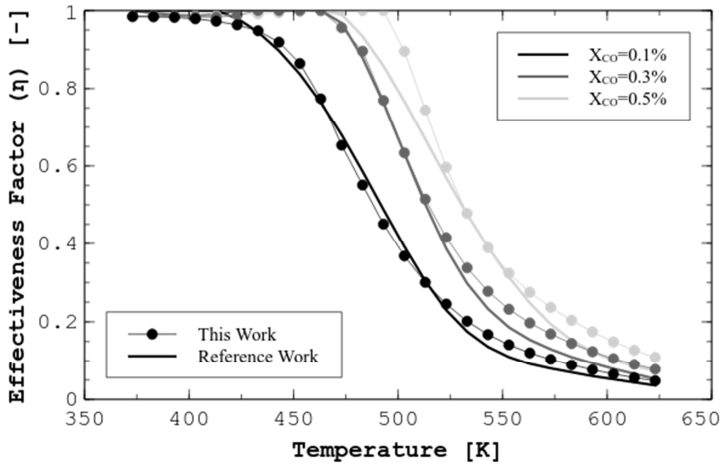

Fig. 4 – Effectiveness factors obtained in this work and reported in the literature for similar operating conditions. Operating conditions: ${X_{O_2}}^{bnd} = 2\%$, ${X_{CO_2}}^{bnd} = {X_{CO}}^{bnd} = \{0.1;\ 0.3;\ 0.5\}\%$ and N_2 to balance.

Results

The washcoat sample considered in this study has a bimodal pore structure with the mesoporous structure reconstructed following the parameters listed in Table 1 and with a macroporous structure generated considering the parameters presented in Table 2. The macroporous geometry is composed by spheres of two different diameters with a specific mixing ratio (grain size distribution).

Table 2 – Structural parameters required for the digitally reconstruction of the macroporous structure (micro-scale physical model).

Structural Parameter	Value
Sphere 1 Diameter ($d_{s_1}^{M}$)	5 μm
Sphere 2 Diameter ($d_{s_2}^{M}$)	1.2 μm
Mixing Ratio ($s_1 : s_2$)	1 : 16
Porosity (ε^{M})	18%
Exclusion Factor (F_E)	0.8
System Size ($L_x \times L_y \times t$)	$10 \times 10 \times 50$ μm^3

Fig. 5 presents CO effective diffusion coefficients in the mesoporous and in the overall layer calculated through 3D multi-scale diffusion simulations and through the random pore model. In the temperature range considered (298 K – 623 K) and for the current porous sample, the random pore model underestimates the effective diffusion coefficients predicted by the 3D multi-scale diffusion model by about 32% to 35%.

The influence of the method employed to evaluate the effective diffusion coefficients for the 1D reaction-diffusion model is investigated in Fig. 6 at the washcoat level. In particular, Fig. 6a presents the effectiveness factor values computed through the 3D multi-scale methodology. Increasing the system temperature a significant decrease of the effectiveness factor is observed independently of the surface mixture composition. In fact, this effect (a significant loss on the effectiveness factor and consequently on the washcoat utilization) is more pronounced varying the temperature than varying the external mixture composition in the ranges considered. The operating conditions that lead to an increase of the surface chemistry rates in relation to the rates of species transport also lead to a decrease of the effectiveness factor. Therefore, increasing the layer temperature and CO content on the external layer surface a decrease of the effectiveness factor is observed as Fig. 6a shows.

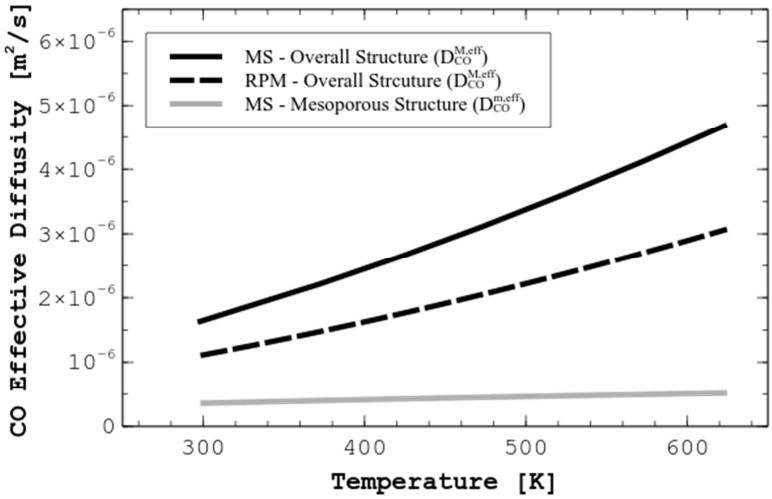

Fig. 5 – CO effective diffusion coefficients calculated through the multi-scale methodology (MS), in the nano- and micro-scale levels, and predicted with the random pore model (RPM).

Figs. 6b and 6c present the comparisons between the performance of the 3D multi-scale approach and the 1D reaction-diffusion model considering two strategies to evaluate the required effective transport data for the 1D model: the RPM (1D-RPM) and the 3D multi-scale diffusion model (1D-MS) – Figs. 6b and 6c, respectively. For both techniques of computing effective diffusivities the results are closer to the 3D effectiveness factor values in the region without diffusional limitations (for low temperatures) as it would be expected since in this region the actual values for effective diffusivities are somewhat irrelevant due to the irrelevance of the surface kinetic

rates. Conversely, for high temperatures and mixtures with high CO concentrations, the differences between both strategies to computed effective diffusion coefficients are more striking. In particular, as the comparison between Figs. 6b and 6c suggests, the evaluation of effective transport data for the 1D reaction-diffusion model through the 3D multi-scale approach allows to obtain a performance closer to the performance predicted by the 3D multi-scale reaction-diffusion model.

The effect of the source (model) for the effective transport data on the performance of full-scale reactor model is further analyzed through the application of the 1D heterogeneous single-channel model. The physical model of the reactor is presented in Fig. 7. The reactor is composed by three main regions: the front heat shield, the catalyst and the back heat shield. All three reactor regions are composed by square-shaped channel 600/6.7 cordierite honeycomb monoliths. The heat shields have no catalyst activity and their main purpose consists in preventing radiative heat losses from the catalyst monolith in order to ensure the axial adiabaticity of the whole reactor. Negligible heat losses from the reactor through the lateral reactor walls (reactor housing) are also considered.

Table 3 lists the geometrical and thermophysical properties required for the 1D full-scale heterogeneous model. The catalytic volumetric fraction was calculated through Eq. (14) considering no rounded corners after the washcoat application. In Eq. (14), L corresponds to the cell pitch and t corresponds to the washcoat thickness applied onto the cordierite substrate walls. The washcoat thickness is equal to 50 µm, as considered before in Table 2.

$$\xi = \frac{4t(d_h + t)}{L^2} \tag{14}$$

The coupling between the washcoat models (3D-MS, 1D-MS and 1D-RPM) and the full-scale reactor model is carried out by pre-computing the averaged reaction rates with the three reaction-diffusion models for a specific range of temperature, CO and O_2 mole fractions and then interpolating such data, applying cubic splines, during the numerical solution procedure of the full-scale reactor model.

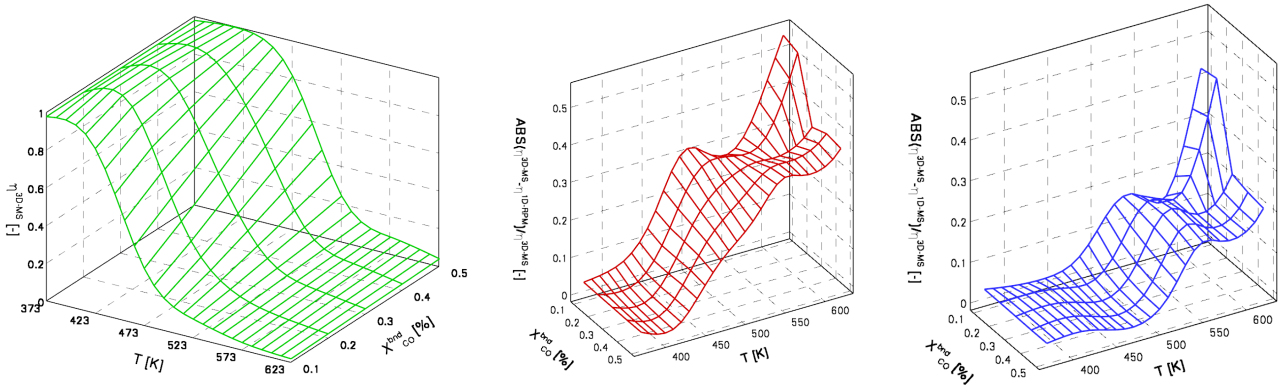

Fig. 6 – Effectiveness factor values computed with the 3D multi-scale model (a) and comparison with the 1D pseudo-homogeneous reaction-diffusion models: with effective diffusivities computed with the RPM (b) and through multi-scale diffusion simulations (c). $X_{O_2}{}^{bnd} = 2\%$, $X_{CO_2}{}^{bnd} = X_{CO}{}^{bnd}$ and N_2 to balance.

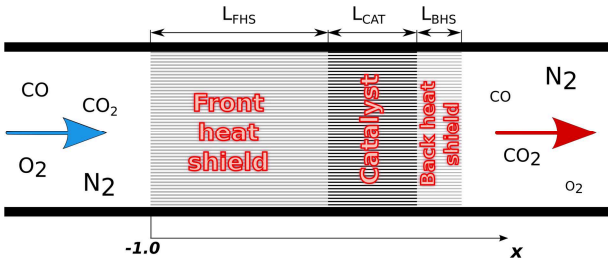

Fig. 7 – Physical model of the honeycomb monolith reactor. $L_{FHS} = 4$ cm; $L_{Cat} = 2$ cm and $L_{BHS} = 1$ cm.

Table 3 – Geometrical and thermophysical properties of the honeycomb reactor.

Property	Value
Hydraulic Diameter (d_h)	0.0868 mm
Porosity (ε)	70%
Specific Surface Area (a_V)	3.23 mm^{-1}
Catalytic Volumetric Fraction (ξ)	17%
Effective Thermal Conductivity ($k_{s,eff}$)	3.0 $W.m^{-1}.K^{-1}$

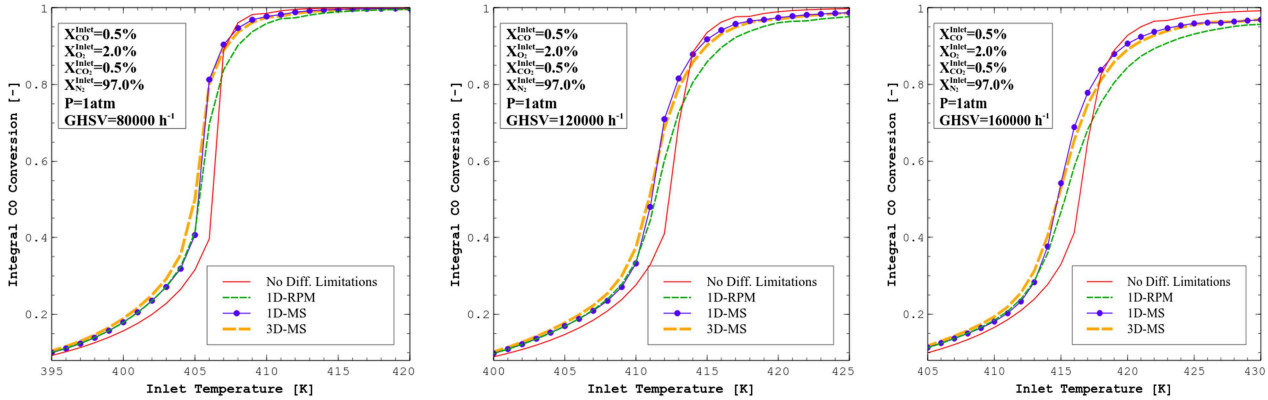

(a) **(b)** **(c)**

Fig. 8 – Integral CO conversion as a function of the inlet gas temperature for three different total volumetric flow rates: (a)GHSV = 80000 h^{-1}; (b) GHSV = 120000 h^{-1}; (c) GHSV = 160000 h^{-1}.

Fig. 8 presents fractional conversion profiles for CO at the outlet section of the reactor (x = 6 cm) for three different gas hourly space velocities (GHSV). Gas hourly space velocities were computed on the basis of the total catalyst volume and defined at the standard temperature and pressure of 298 K and 1 atm, respectively. As the gas hourly space velocity increases the light-off temperature (inlet gas temperature for which the CO conversion reaches a value equal to 50%) increases for all the four cases: 1) without diffusional limitations ("No Diff. Limitations"); 2) 1D-RPM; 3) 1D-MS and 4) 3D-MS. Moreover, increasing the total volumetric flow rate the transition from low to high conversion values becomes smoother.

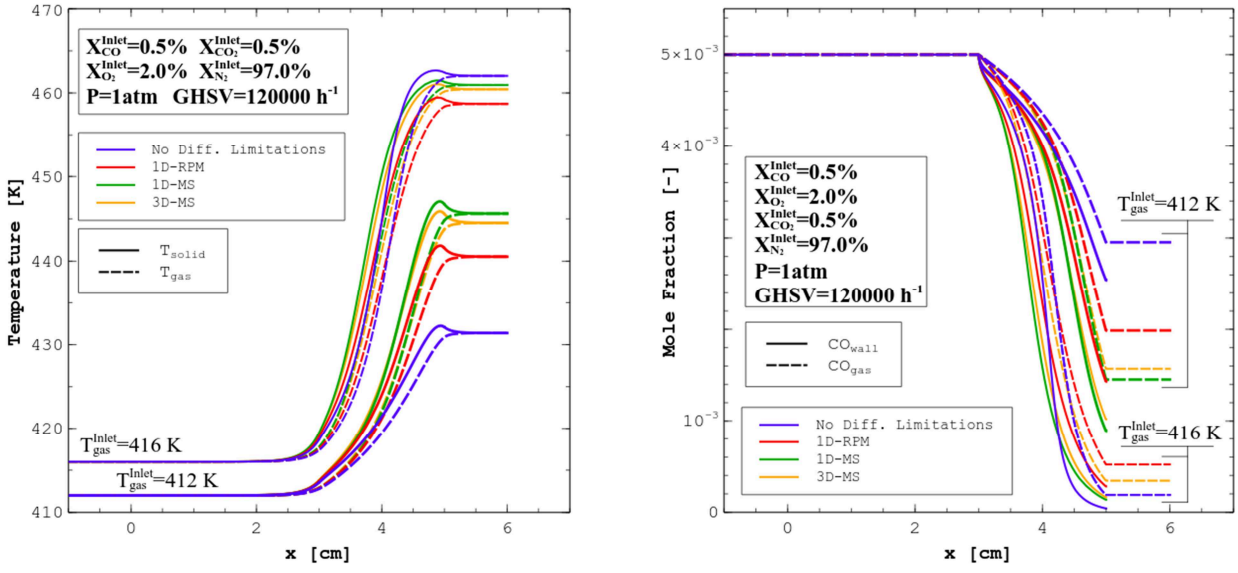

(a) **(b)**

Fig. 9 – Performance of the honeycomb reactor for two inlet gas temperatures (412 K and 416 K) considering different strategies to take into account internal diffusional limitations: a) solid and gas temperature profiles; b) CO product distribution profiles at the wall and in the bulk gas flow.

For the three GHSV values considered at low inlet gas temperatures (lower temperatures than the light-off temperature) higher values for CO conversion are registered by considering transport limitations in the model along the catalytic layer. This is justified on the basis of the CO self-inhibition effect taken into account in the surface chemistry rate expression because the kinetic rate may not increase by increasing the CO concentration (see reference [2]). Therefore, in the three cases that consider intraphase diffusion limitations, a CO concentration gradient is observed along the catalyst layer for each reactor axial location and lower values of CO mole fraction are registered along the layer thickness increasing locally the rates species consumption/production and resulting in an increase in the averaged (observed) reaction rate. For high temperatures the effectiveness factor has low values (see Fig. 6a) and as a result higher CO conversion values are attained for negligible mass transport resistances in the washcoat layer.

In Figs. 8a, 8b and 8c it is clear that the CO conversion results computed with the 1D-MS model are closer to the 3D-MS results than the results predicted by the 1D-RPM model. This is particularly remarkable for high inlet gas temperatures. The lower conversion values predicted by the 1D-RPM in relation to the values of the 3D-MS and 1D-MS models are in line with the underestimation of the effective diffusion coefficients computed with the random pore model in relation to the results of the 3D multi-scale diffusion model (see Fig. 5).

Fig. 9 shows the axial reactor performance for two different inlet gas temperatures (412 and 416 K) which for the considered total volumetric flow rate (GHSV=120000 h^{-1}), total pressure and inlet mixture composition correspond to two operating regimes around the light-off point. In particular, Fig. 9a presents the solid and gas thermal profiles and Fig. 9b presents the mole fraction profiles of CO at the wall and in the bulk gas flow. For both inlet temperatures the results predicted with the 1D-MS model are in good agreement with the results calculated with the 3D-MS strategy.

The good agreement observed between the full-scale reactor model results computed with the 3D-MS and with the 1D-MS washcoat models reinforces the suggestion reported in a previous work by the authors [18] related with the advantage of employing the 1D-MS instead of the 3D-MS in terms of computational cost. Computational time savings with the 1D-MS strategy become even more remarkable for reaction schemes depending on several parameters to compute all rate-of-progress variables (in this work only three variables – layer temperature, CO and O_2 mole fractions – were considered for the kinetic rates evaluation).

Conclusions

In this work a multi-scale bottom-up approach was considered for modeling diffusion and reaction-diffusion in porous layers. An underprediction in the range 32-35% on the effective diffusivity values was observed with the random pore model regarding the results computed with the multi-scale diffusion model. Three strategies to pre-compute intraporous transport resistances for a full-scale reactor model were considered: (a) 3D multi-scale reaction diffusion model; (b) 1D pseudo-homogeneous reaction-diffusion model with effective transport data from the application of the random pore model and (c) 1D pseudo-homogeneous reaction-diffusion model with effective transport data evaluated with the 3D multi-scale diffusion model. The strategy (c) has shown significant advantages in terms of computational time savings at the expense of a small solution error in relation to option (a). The technique (b) presents the worst results for the full-scale reactor performance mainly due to the predictive capability of the random pore model formulation.

Acknowledgments. This work was partially funded by the European Commission within the 7th FP (260105 FC-DISTRICT).

References

[1] M. V. Twigg: Catalysis Today Vol. 163 (2011), p. 33
[2] S. E. Voltz, C. R. Morgan, D. Liederman and S. M. Jacob: Ind. Eng. Chem. Prod. Res. Develop. Vol. 12 (1973), p. 294
[3] G. B. Froment and K. B. Bischoff: *Chemical Reactor Analysis and Design* (John Wiley & Sons, New York 1990).
[4] J. Chen, H. Yang, N. Wang, Z. Ring and T. Dabros: Appl Catal A Gen Vol. 345 (2008), p. 1
[5] N. Mladenov, J. Koop, S. Tischer and O. Deutschmann: Chem Eng Sci Vol. 65 (2010), p. 812
[6] D. Leung, R. E. Hayes and S. T. Kolaczkowski: Can J Chem Eeng Vol. 74 (1996), p. 94 [7] M. Pacheco, J. Sira and J. Kopasz: Appl Catal A Gen Vol. 250 (2003), p. 161
[8] R. E. Hayes, B. Liu and M. Votsmeier: Chem Eng Sci Vol. 60 (2005), p. 2037
[9] A. P. Roberts: Phys Rev E Vol. 56 (1997), p. 3203
[10] F. Ŝtěpánek and M. A. Ansari: Chem Eng Sci Vol. 60 (2005), p. 4019
[11] R. Moreno-Atanasio, R. A. Williams and X. Jia: Particuology Vol. 8 (2010), p. 81
[12] P. Kočí, F. Ŝtěpánek, M. Kubíček and M. Marek: Chem Eng Sci Vol. 62 (2007), p. 5380
[13] J. Becker, C. Wieser, S. Fell and K. Steiner: Int J Heat Mass Tran Vol. 54 (2011), p. 1360
[14] M. Dudák, V. Novák, P. Kočí M. Marek, P. Blanco-García and G. Jones: Appl Catal B Environ Vol 150-151 (2014), p. 446
[15] N. Zamel, J. Becker and A. Wiegmann: J Power Sources Vol. 207 (2012), p. 70
[16] A. T. Naseri, B. A. Peppley and J. G. Pharoah: AIChE J Vol. 60 (2014), p. 2263
[17] V. Novák, P. Kočí, F. Ŝtěpánek and M. Marek: Ind Eng Chem Res Vol. 50 (2011), p. 12904
[18] J. M. C. Pereira, J. E. P. Navalho, A. C. G. Amador and J. C. F. Pereira: Chem Eng Sci Vol. 117 (2014), p. 364
[19] V. Novák, F. Ŝtěpánek, P. Kočí, M. Marek and M. Kubíček: Chem Eng Sci Vol. 65 (2010), p. 2352
[20] B. E. Poling and J. M. Prausnitz and J. P. O'Connel: *The Properties of Gases and Liquids* (McGraw-Hill, New York 2001).
[21] N. Wakao and J. M. Smith: Chem Eng Sci Vol. 17 (1962), p. 825
[22] J. E. P. Navalho, I. Frenzel, A. Loukou, J. M. C. Pereira, D. Trimis and J. C. F. Pereira: Int J Hydrogen Energ Vol. 38 (2013), p. 6989
[23] J. E. P. Navalho, J. M. C. Pereira and J. C. F. Pereira: Int J Hydrogen Energ Vol. 39 (2014), p. 3666
[24] J. E. P. Navalho: *Modeling and Simulation of Catalytic Partial Oxidation in Monolith Reactors* (MSc Thesis, Instituto Superior Técnico, Lisboa 2013)
[25] L. O. E. dos Santos, P. C. Philippi, C. P. Fernandes and H. C. de Gaspari, in: Proceedings of the ENCIT (2002)

Recent Developments of Diffusion Processes and their Applications: Fluid, Heat and Mass
10.4028/www.scientific.net/DDF.364

Multi-Scale Modeling of Internal Mass Diffusion Limitations in CO Oxidation Catalysts
10.4028/www.scientific.net/DDF.364.92

DOI References

[1] M. V. Twigg: Catalysis Today Vol. 163 (2011), p.33.
http://dx.doi.org/10.1016/j.cattod.2010.12.044
[2] S. E. Voltz, C. R. Morgan, D. Liederman and S. M. Jacob: Ind. Eng. Chem. Prod. Res. Develop. Vol. 12 (1973), p.294.
http://dx.doi.org/10.1021/i360048a006
[4] J. Chen, H. Yang, N. Wang, Z. Ring and T. Dabros: Appl Catal A Gen Vol. 345 (2008), p.1.
http://dx.doi.org/10.1016/j.apcata.2008.04.010
[5] N. Mladenov, J. Koop, S. Tischer and O. Deutschmann: Chem Eng Sci Vol. 65 (2010), p.812.
http://dx.doi.org/10.1016/j.ces.2009.09.034
[6] D. Leung, R. E. Hayes and S. T. Kolaczkowski: Can J Chem Eeng Vol. 74 (1996), p.94.
http://dx.doi.org/10.1002/cjce.5450740112
[7] M. Pacheco, J. Sira and J. Kopasz: Appl Catal A Gen Vol. 250 (2003), p.161.
http://dx.doi.org/10.1016/S0926-860X(03)00291-6
[9] A. P. Roberts: Phys Rev E Vol. 56 (1997), p.3203.
http://dx.doi.org/10.1103/PhysRevE.56.3203
[10] F. Ŝtěpánek and M. A. Ansari: Chem Eng Sci Vol. 60 (2005), p.4019.
http://dx.doi.org/10.1016/j.ces.2005.02.030
[11] R. Moreno-Atanasio, R. A. Williams and X. Jia: Particuology Vol. 8 (2010), p.81.
http://dx.doi.org/10.1016/j.partic.2010.01.001
[12] P. Kočí, F. Ŝtěpánek, M. Kubíček and M. Marek: Chem Eng Sci Vol. 62 (2007), p.5380.
http://dx.doi.org/10.1016/j.ces.2006.12.033
[13] J. Becker, C. Wieser, S. Fell and K. Steiner: Int J Heat Mass Tran Vol. 54 (2011), p.1360.
http://dx.doi.org/10.1016/j.ijheatmasstransfer.2010.12.003
[15] N. Zamel, J. Becker and A. Wiegmann: J Power Sources Vol. 207 (2012), p.70.
http://dx.doi.org/10.1016/j.jpowsour.2012.02.003
[16] A. T. Naseri, B. A. Peppley and J. G. Pharoah: AIChE J Vol. 60 (2014), p.2263.
http://dx.doi.org/10.1002/aic.14411
[17] V. Novák, P. Kočí, F. Ŝtěpánek and M. Marek: Ind Eng Chem Res Vol. 50 (2011), p.12904.
http://dx.doi.org/10.1021/ie2003347
[18] J. M. C. Pereira, J. E. P. Navalho, A. C. G. Amador and J. C. F. Pereira: Chem Eng Sci Vol. 117 (2014), p.364.
http://dx.doi.org/10.1016/j.ces.2014.06.028
[19] V. Novák, F. Ŝtěpánek, P. Kočí, M. Marek and M. Kubíček: Chem Eng Sci Vol. 65 (2010), p.2352.
http://dx.doi.org/10.1016/j.ces.2009.09.009
[21] N. Wakao and J. M. Smith: Chem Eng Sci Vol. 17 (1962), p.825.
http://dx.doi.org/10.1016/0009-2509(62)87015-8
[22] J. E. P. Navalho, I. Frenzel, A. Loukou, J. M. C. Pereira, D. Trimis and J. C. F. Pereira: Int J Hydrogen Energ Vol. 38 (2013), p.6989.

http://dx.doi.org/10.1016/j.ijhydene.2013.02.141
[23] J. E. P. Navalho, J. M. C. Pereira and J. C. F. Pereira: Int J Hydrogen Energ Vol. 39 (2014), p.3666.
http://dx.doi.org/10.1016/j.ijhydene.2013.12.107